Solar Energy Materials & Solar Cells 101 (2012) 73–78

Contents lists available at SciVerse ScienceDirect

Solar Energy Materials & Solar Cells

journal homepage: www.elsevier.com/locate/solmat

Disordered submicron structures integrated on glass substrate for broadband absorption enhancement of thin-film solar cells

Young Min Song [a], Ji Hoon Jang [b], Jeong Chul Lee [b], Eun Kyu Kang [a], Yong Tak Lee [a,c,d,*]

[a] Department of Information and Communications, Gwangju Institute of Science and Technology, Gwangju 500-712, Korea
[b] KIER-UNIST Advanced Center for Energy, Korea Institute of Energy Research, Daejeon 305-343, Korea
[c] Department of Nanobio Electronics and Materials, Gwangju Institute of Science and Technology, Gwangju 500-712, Korea
[d] Graduate Program of Photonics and Applied Physics, Gwangju Institute of Science and Technology, Gwangju 500-712, Korea

ARTICLE INFO

Article history:
Received 19 January 2012
Accepted 13 February 2012

Keywords:
Solar cell
Disordered submicron structures
Antireflective characteristics
Nanoparticles
Silicon
Rigorous coupled wave analysis

ABSTRACT

We report the effect of antireflective disordered submicron structures (d-SMSs) on glass substrates for the absorption enhancement of thin-film solar cells. The shape and height of d-SMSs were designed on the basis of the calculation result from the rigorous coupled wave analysis (RCWA) method. The d-SMSs with tapered shape were fabricated on the back side of SnO_2:F covered glass substrate by plasma etching of thermally dewetted silver (Ag) nanoparticles without any lithography processes. The glass substrates with d-SMSs showed very low reflectance compared to that of the glass substrates with flat surface over a wide specular and angular range. Thin-film hydrogenated amorphous silicon (a-Si:H) solar cells were prepared on the opposite side of d-SMSs integrated glass substrates, and the devices exhibited a short-circuit current density (J_{sc}) of 6.84% increased value compared to the reference cells with flat surface without detrimental changes in the open circuit voltages (V_{oc}) and fill factor. Also, it is found that the performance of the solar cells is sustained over a wide incident angle of light.

1. Introduction

Thin-film solar cells made from various semiconductors or organic materials have great potential for the next generation of photovoltaic applications due to their low material cost and easy fabrication, which are ideal for large-scale manufacturing [1–3]. However, the relatively thin photoactive layer does not absorb light effectively, resulting in poor cell performance. In order to improve light absorption in thin-film solar cells, it is essential to reduce the reflection at the top surface of solar cells in the entire light absorbing spectra. For the so-called superstrate type thin-film solar cells, where the active cells are deposited onto a transparent glass covered by transparent conducting oxide (TCO), the reflection at the interface between air and glass should be minimized. Antireflection coatings (ARCs) have been commonly used on the top surface of the device for the antireflection purpose, but it can give zero reflection at only specific wavelength ranges. Moreover, to fulfill the phase matching condition for the interface between air ($n_{air}=1$) and a typical glass (assumption $n_{glass}=1.5$), the refractive index of the ARC layer has to be $n_{ARC}\sim 1.22$, which is not available for thin-film materials.

Recently, submicron structures (SMSs), which are inspired by a corneal of night active insects such as a moth or a mosquito, have been focused on as a more practical method instead of the conventional ARCs for broadband and omni-directional antireflection [4–11]. On the basis of the effective medium theory, for the broadband AR performance, the structures should have, at the same time, a tapered profile and a size smaller than the incident wavelength. Furthermore, the height should be as tall as possible to cover a broader range of wavelengths [5]. However, due to the difficulties of fabricating structure with high aspect ratio (i.e., height/period) on real devices, such kinds of antireflective nanostructures should be optimized to specific regions of wavelengths for practical applications. Despite great efforts to produce the antireflective SMSs on organic/inorganic materials in various ways, there have been only a few studies reported on thin-film solar cells integrated with antireflective SMSs. In this work, we fabricated disordered SMSs (d-SMSs) with thermally dewetted Ag nanoparticles (NPs) on top of the superstrate type thin-film hydrogenated amorphous silicon (a-Si:H) solar cells to improve the light absorption. Thermal dewetting process of thin metal films provides nanoscale mask patterns without lithography process, which enables cost effective fabrication [12–14]. The theoretical calculation based on the rigorous coupled-wave analysis (RCWA) method was utilized for the guidance of geometrical effect of d-SMSs. The antireflective properties of d-SMSs were investigated by reflectance spectra measurement and confirmed

* Corresponding author at: Gwangju Institute of Science Technology, Department of Information and Communications, Gwangju 500-712, Korea.
E-mail address: ytlee@gist.ac.kr (Y.T. Lee).

0927-0248/$ - see front matter © 2012 Elsevier B.V. All rights reserved.
doi:10.1016/j.solmat.2012.02.013

by the characterization of the fabricated solar cells. The angle dependence of antireflection performance was also studied.

2. Experimental details

Fig. 1 illustrates the basic structure of thin-film a-Si:H solar cells integrated with antireflective d-SMSs. As shown in Fig. 1, the d-SMSs are fabricated on the glass's surface to provide broadband antireflection. The steps in the d-SMSs fabrication are depicted in the left image of Fig. 1. The process begins with an Asahi VU glass substrate covered with textured SnO_2:F film on one surface, which is then turned over to deposit an Ag thin-film with an e-beam evaporator on the opposite side. The Ag thin-film thickness and evaporation rate were 20 nm and 0.05 nm/sec, respectively. Prior to depositing the Ag film, the glass substrate was first cleaned with ultrasonic agitation in acetone and methanol, followed by rinsing with distilled water. To form Ag NPs, the samples were heated in a rapid thermal annealing (RTA) system at 500 °C for 1 min in a nitrogen environment. During the RTA process, the Ag thin-film breaks up into NPs via the dewetting mechanism [12]. To fabricate d-SMSs with a tapered profile, an overall dry etch process was carried out using an inductively coupled plasma reactive ion etch (ICP-RIE) system in a SF_6/O_2 (40 sccm/10 sccm) gas mixture at room temperature. The process pressure, RF power, and ICP power were kept at 20 mTorr, 100 W, and 200 W, respectively. To remove the residual Ag NPs, the samples were dipped into $KI/I_2/H_2O$ (1 g/1 g/40 ml) solution for 10 sec. Surface morphology of the fabricated d-SMSs on glass substrate was characterized by a field-emission scanning electron microscope (FE-SEM, Hitachi S-4700). The reflectance spectra were evaluated using a spectrophotometer (Cary 500, Varian) with an integrating sphere. For angle dependent reflectance measurement, a variable angle reflectance accessory was used in specular mode.

For the fabrication of thin-film a-Si:H solar cells with d-SMSs, p-i-n structured a-Si:H cells were deposited on the opposite side of the d-SMSs integrated SnO_2:F covered glass. All of these steps were performed using the multi-chamber plasma-enhanced chemical vapor deposition (PECVD) system. As depicted in Fig.1, the solar cells were composed of d-SMSs integrated glass/SnO_2:F/p-i-n cells/Ag back reflector. Each thin film was prepared separately in isolated chambers to prevent cross contamination. Boron-doped a-SiC:H with a thickness of 20 nm and phosphorus-doped a-Si:H with a thickness of 30 nm were deposited in a 13.56 MHz RF PECVD at 200 °C. The 200 nm-thick intrinsic a-Si:H layers were deposited with a 60 MHz very high frequency chemical vapor deposition (VHFCVD). Ag backside metal reflector (300 nm) was coated by a thermal evaporator. The device area was defined to 0.25 cm^2 by Ag metal area, and conventional thin-film a-Si:H solar cells with flat glass surface were also fabricated for comparison. Current density-Voltage (J–V) characteristics of the solar cells were measured by using a solar simulator (WACOM, AM 1.5 G, 1 sun) at room temperature. External quantum efficiency of the cells was also measured by incident photon to charge carrier efficiency (IPCE, PV measurements Ltd.) in the wavelength range of 300–900 nm.

3. Results and discussion

According to theoretical studies, a more gradual transition of the refractive index leads to a smaller surface reflection. This indicates that in order to maximize antireflective properties of the SMS surfaces, high aspect ratio SMS arrays with a gradually changed diameter such as nanotip arrays with a tip height of above 1 μm are highly desired [5]. However, it is difficult to attain such features on glass substrates with conventional dry/wet etch techniques. Consequently, it is crucial to determine an optimum geometry of SMSs in a given height. Fig. 2 shows the calculated reflectance of (a) cone- and (b) truncated cone-shaped SMSs with a period of 300 nm as a function of the SMS height at three different wavelengths (i.e., λ=300 nm, 550 nm, and 800 nm). These calculations were implemented by a three-dimensional RCWA method, and for simplicity, structures with a closely packed six-fold hexagonal symmetry were used instead of disordered structures as shown in insets of Fig. 2. In the truncated cone, the apex diameter was set to 50% of the base diameter. The flat surface (i.e., height=0) of glass exhibits the reflectance of ~4.0% at 300 nm wavelength, and this value slightly decreases as the wavelength increases due to the material dispersion. As the height increases, the reflectance tends to decrease, which results from the gradually changing effective refractive index. The cone-shaped SMSs are more favorable to obtain low reflectance than the truncated cone at taller heights. However, below ~200 nm height, the truncated cone shows lower reflectance at a visible wavelength range. For example, the minimum heights of truncated cone-shaped

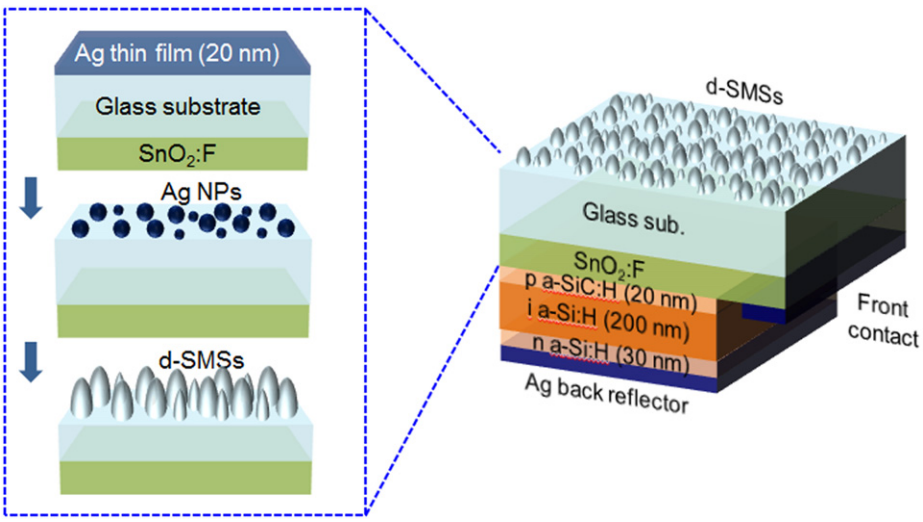

Fig. 1. Schematic illustration of thin-film amorphous silicon (a-Si) solar cells with disordered submicron structures (d-SMSs) for broadband antireflection. The inset on the left shows the fabrication procedure for d-SMSs by using thermally dewetted silver nanoparticles (NPs).

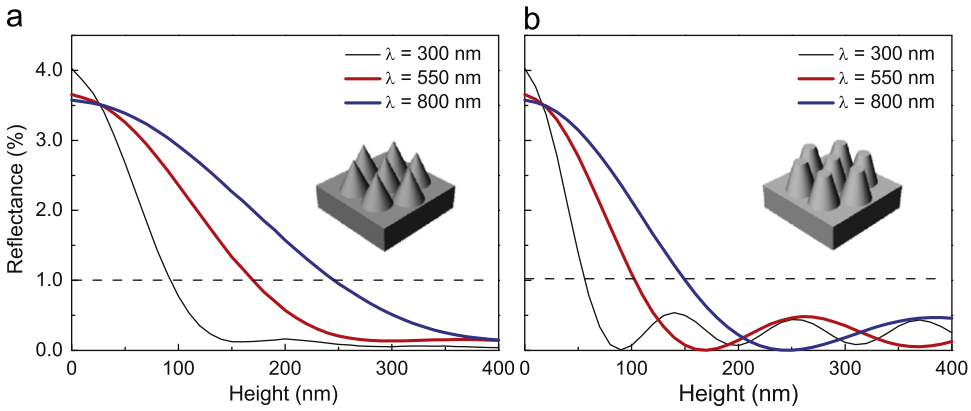

Fig. 2. Calculated reflectance of d-SMSs with (a) cone shape and (b) truncated cone shape as a function of heights (0–400 nm) at three different incident wavelengths.

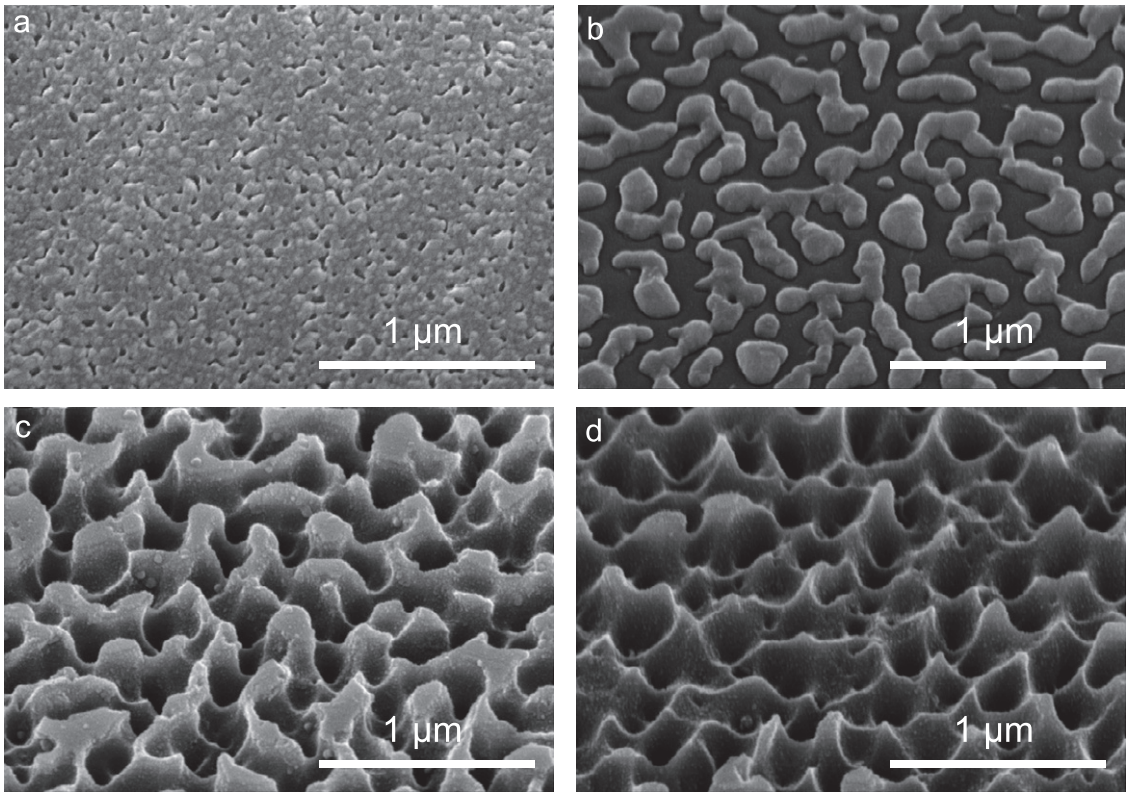

Fig. 3. Scanning electron microscope images of (a) as deposited Ag thin film on glass substrate, (b) Ag NPs thermally dewetted at 500 °C for 1 min, (c)–(d) fabricated d-SMSs by dry etch of Ag NPs in ICP-RIE for (c) 7 min and (d) 9 min, respectively.

SMSs to obtain below 1% reflectance are 55 nm, 102 nm, and 150 nm at wavelength of 300 nm, 550 nm, and 800 nm, respectively, whereas those of cone-shaped SMSs are 92 nm, 170 nm, and 225 nm. This indicates that the rapid change of the effective refractive index rather obstructs the reduction of reflection in cone shaped SMSs. This anticipation can be applied to disordered structures; if the d-SMSs have sharp apexes with below 200 nm heights, then the reflectance will not be lowered than that of d-SMSs with a truncated shape.

Fig. 3 shows scanning electron microscope images of Ag thin-films on glass substrate (a) as deposited with a thickness of 20 nm and (b) annealed at 500 °C for 1 min under a nitrogen atmosphere. Because the surface energy of Ag film is much higher than glass, the former is unstable on glass substrates, resulting in dewetting of the film with the annealing process. By controlling the process conditions, such as RF power, gas mixture, and process time, during an overall dry etch of Ag NPs, various shaped nanostructures can be fabricated. In this experiment, cone- and truncated cone-shaped SMSs were prepared by changing the process time. As shown in Figs. 3(c) and (d), as etch time increases from 7 min to 9 min, the shape of d-SMS converts from truncated cone to cone, which results from a mask erosion effect. Because the fabricated d-SMSs show bicontinous shapes, it is difficult to characterize the average distance of each cone. However, this can be roughly estimated by counting the number of apex within unit distance. In our structures, the average distance of each cone is between 300–400 nm, which value

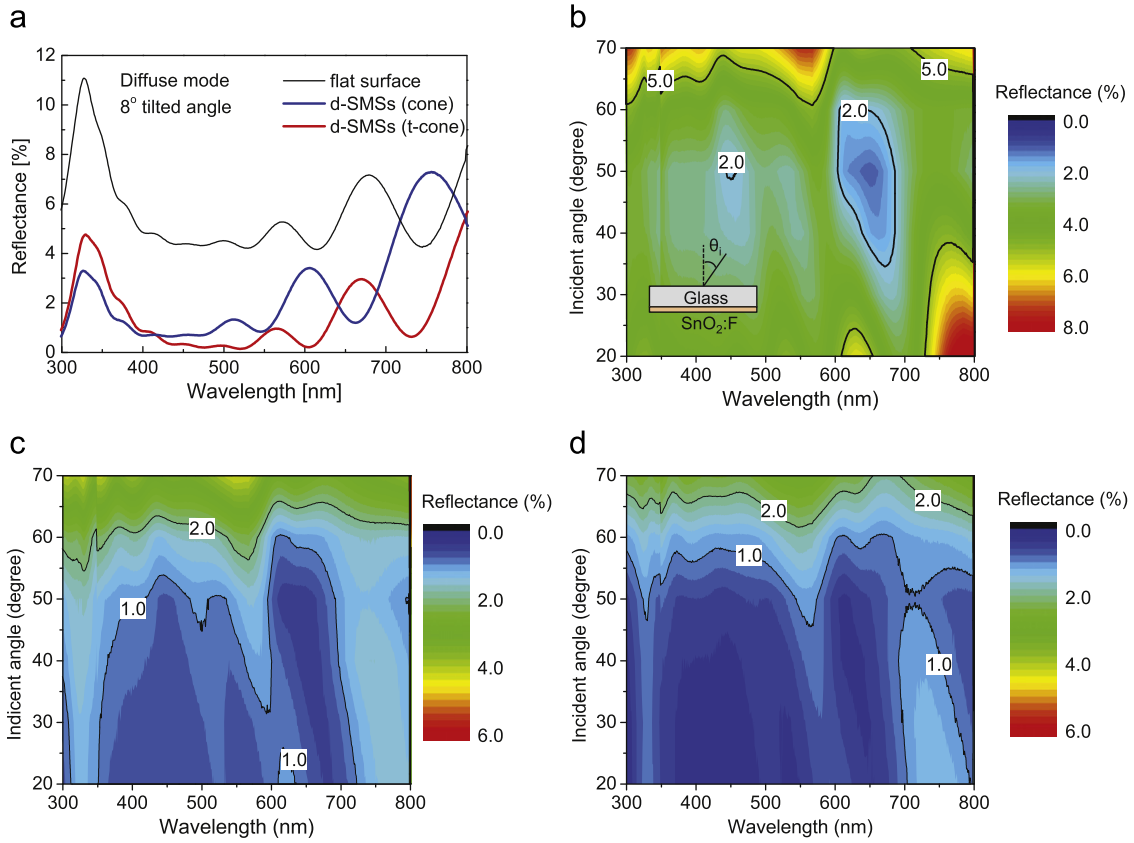

Fig. 4. (a) Measured reflectance of three different type glass substrate (flat surface, cone shaped d-SMSs, and truncated cone shaped d-SMSs) in diffuse mode. (b)–(d) Contour plots for angle dependent reflectance spectra of glass substrate with (b) flat surface, (c) cone shaped d-SMSs, and (d) truncated cone shaped d-SMSs at incident angles of 20°–70° in specular mode. The inset in (b) shows a schematic of the measurement setup.

is reasonable for broadband antireflection in thin film solar cells [11,15].

Fig. 4(a) shows the measured reflectance of d-SMSs with cone and truncated cone shape on glass/SnO_2:F substrate in diffuse mode with 8° tilted angle. For comparison, the reflectance of bulk glass/SnO_2:F with flat surface is also shown in Fig. 4(a), exhibiting values 4∼11% at wavelengths of 300–800 nm. The reflectance was drastically reduced for both d-SMSs in whole visible wavelength ranges, and as expected in calculations, the d-SMSs with truncated cone shape show lower reflectance spectra than the cone-shaped d-SMSs. The average reflectance of truncated-cone-shaped SWSs was 1.52% in the wavelength range of 300–800 nm, while that of cone-shaped SWSs was 2.54%. Figs. 4(b)-(d) shows the contour plots of the reflectance variation as a function of wavelength (300–800 nm) and incident angle (20–70°) for three different type glass substrate (flat surface, cone-shaped d-SMSs, and truncated-cone-shaped d-SMSs). Because of the back scattering of incident light at textured SnO_2:F surfaces, the angle dependent reflectance, measured in specular mode, is slightly lower than the total reflectance presented in Fig. 4(a). In all cases, the reflectance increases as the incident angle increases, but as shown in Figs. 4(c) and (d), relatively lower reflectance is sustained at high incident angle in the d-SMSs. In particular, the d-SMSs with truncated cone shape reduce fairly better the reflectance over a wide spectral and angular range.

The influence of the d-SMSs on solar cell performance is revealed in Fig. 5. Fig. 5(a) represents the current density-voltage (J–V) curves of the solar cells with and without d-SMSs. In this experiment, we applied the d-SMSs with truncated cone shape on the top of thin-film a-Si:H solar cells for better antireflection. The obtained device characteristics are summarized in Table 1. The a-Si:H solar cells with d-SMSs exhibits a short-circuit current density (J_{sc}) of 6.84% increased value compared to the reference cells with flat surface, while the open circuit voltages (V_{oc}) and fill factor are kept as similar values. Because the d-SMSs are electrically separated from the p-i-n structured a-Si:H cells, the electrical properties are not affected by the d-SMSs. The effect of the incident angle of light on the efficiency of a solar cell is crucial for device performance. Fig. 5(b) shows the normalized current density (i.e., $J_{sc}(\theta_i)/J_{sc}(0^\circ)$) of a-Si:H solar cells as a function of the incident angle. The J_{sc} of solar cells with flat surface drops rapidly as the incident angle increases due to the increased reflection loss. In the d-SMSs integrated solar cells, however, the rapid drop of the J_{sc} is released, which results from the angle-independent antireflection characteristics of the d-SMSs. Fig. 5(c) shows the spectra of external quantum efficiency (EQE) measured with the two different solar cells. The EQE for the d-SMSs integrated solar cells is improved at entire light absorbing ranges. This observation echoes with the reflection spectra in Fig. 4, where it shows broadband antireflection. As shown in Fig. 4(d), the enhancement ratio of EQE is ∼4% at $\lambda < 550$ nm, and this value increases at longer wavelength regions, which is attributable to the extended optical path length.

4. Conclusion

To enhance the absorption efficiency of superstrate type thin-film solar cells, the d-SMSs were fabricated on glass substrate using the thermally dewetted Ag NPs by the ICP etching and their reflectance characteristics were investigated in terms of wavelength and angle of incidence, together with theoretical

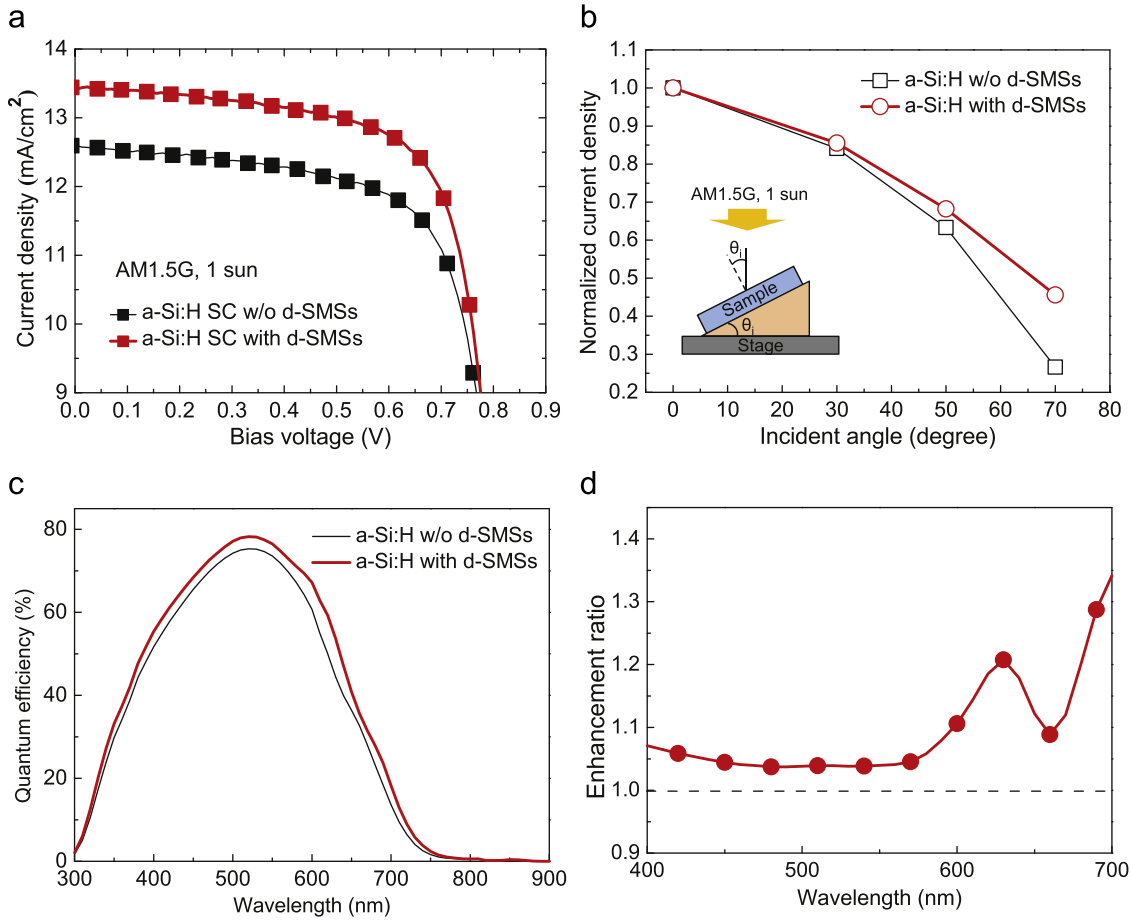

Fig. 5. (a) *J–V* characteristics of thin-film a-Si:H solar cells with and without d-SMSs. (b) Normalized current density ($J_{sc}(\theta_i)/J_{sc}(0^\circ)$) of a-Si:H solar cells as a function of incident angle. Inset: an illustration of the measurement setup. (c) External quantum efficiency of a-Si solar cells with and without d-SMSs. (d) Enhancement ratio of d-SMSs integrated cells against a reference sample with a flat surface.

Table 1
Device characteristics of the a-Si:H solar cells with and without d-SMSs.

	V_{oc} (V)	J_{sc} (mA/cm^2)	Fill Factor (%)	Efficiency (%)
Flat surface	0.85	12.57	70.36	7.49
d-SMSs	0.84	13.43	73.69	8.35

calculation by using RCWA method. The fabricated d-SMSs with truncated cone shape significantly reduced the reflectance compared to the sample with flat surface in visible wavelength ranges. Also, the fabricated thin-film a-Si:H solar cells with d-SMSs showed an increased J_{sc} without any electrical degradation and exhibited enhanced EQE in a whole absorbing region. From these results, we expect that the use of d-SMSs on glass substrate may provide a promising potential for various glass-based thin-film photovoltaic devices.

Acknowledgment

This work was partially supported by the National Research Foundation of Korea (NRF) grant funded by the Korea government (MEST) (no. 2011-0017606), the WCU program at GIST through a grant provided by the MEST of Korea (Project no. R31-20008-000–10026-0), and the Core Technology Development Program for Next-generation Solar Cells of RISE at GIST.

References

[1] H.A. Atwater, A. Polman, Plasmonics for improved photovoltaic devices, Nature Materials 9 (2010) 205–213.
[2] M.A. Green, K. Emery, Y. Hishikawa, W. Warta, E.D. Dunlop, Solar cell efficiency tables (version 39), Progress In Photovoltaics 20 (2011) 12–20.
[3] P. Bermel, C. Luo, L. Zeng, L.C. Kimerling, J.D. Joannopoulos, Improving thin-film crystalline silicon solar cell efficiencies with photonic crystals, Optics Express (2007) 16986-1–16986-5.
[4] Y.M. Song, S.J. Jang, J.S. Yu, Y.T. Lee, Bioinspired parabola subwavelength structures for improved broadband antireflection, Small (Weinheim an der Bergstrasse, Germany) (2010) 984–987.
[5] Y.-F. Huang, S. Chattopadhyay, Y.-J. Jen, C.-Y. Peng, T.-A. Liu, Y.-K. Hsu, C.-L. Pan, H.-C. Lo, C.-H. Shu, Y.-H. Chang, C.-S. Lee, K.-H. Chen, L.-C. Chen, Improved broadband and quasi-omnidirectional anti-reflection properties with biomimetic silicon nanostructures, Nature Nanotechnology 2 (2007) 770–774.
[6] J.W. Leem, Y.M. Song, Y.T. Lee, J.S. Yu, Antireflective properties of AZO subwavelength gratings patterned by holographic lithography, Applied Physics B, Lasers and Optics 99 (2010) 695–700.
[7] Z. Yu, H. Gao, W. Wu, H. Ge, S.Y. Chou, Fabrication of large area subwavelength antireflection structures on Si using trilayer resist nanoimprint lithography and liftoff, Journal Of Vacuum Science and Technology B 21 (2003) 2874–2877.
[8] J. Tommila, V. Polojärvi, A. Aho, A. Tukiainen, J. Viheriälä, J. Salmi, A. Schramm, J.M. Kontio, A. Turtiainen, T. Niemi, M. Guina, Nanostructured broadband antireflection coatings on AlInP fabricated by nanoimprint lithography, Solar Energy Materials and Solar Cells 94 (2010) 1845–1848.
[9] H. Sai, H. Fujii, K. Arafune, Y. Ohshita, M. Yamaguchi, Y. Kanamori, H. Yugami, Antireflective subwavelength structures on crystalline Si fabricated using directly formed anodic porous alumina masks, Applied Physics Letters 88 (2006) 201116-1–201116-3.
[10] W.-L. Min, P. Jiang, B. Jiang, Large-scale assembly of colloidal nanoparticles and fabrication of periodic subwavelength structures, Nanotechnology 19 (2008) 475604-1–475604-7.

[11] Y.M. Song, J.S. Yu, Y.T. Lee, Antireflective submicrometer gratings on thin-film silicon solar cells for light-absorption enhancement, Optics Letters 35 (2010) 276–278.
[12] Y. Kojima, T. Kato, Nanoparticle formation in Au thin films by electron-beam-induced dewetting, Nanotechnology 19 (2008) 255605-1–255605-7.
[13] J.-M. Lee, B.-I. Kim, Thermal dewetting of Pt thin film: Etch-masks for the fabrication of semiconductor nanostructures, Materials Science and Engineering A 449–451 (2007) 769–773.
[14] J.W. Leem, J.S. Yu, Y.M. Song, Y.T. Lee, Antireflective characteristics of disordered GaAs subwavelength structures by thermally dewetted Au nanoparticles, Solar Energy Materials and Solar Cells 95 (2011) 669–676.
[15] J. Li, H.Y. Yu, Y. Li, F. Wang, M. Yang, S.M. Wong, Low aspect-ratio hemispherical nanopit surface texturing for enhancing light absorption in crystalline Si thin film-based solar cells, Applied Physics Letters 98 (2011) 021905-1–021905-3.